DOI: 10.37190/ABB-02529-2024-03

Design and Application of ISSA-BP Neural Network Model for Predicting Soft Tissue Relaxation Force

Yongli Yan[1*], Teng Ren[2], Li Ding[3,1], Tiansheng Sun[4]

[1]Beijing Advanced Innovation Center for Biomedical Engineering, Beihang University, China.

[2]School of Mechanical Engineering, Shenyang University of Technology, China.

[3]School of Biological Science and Medical Engineering, Beihang University, China.

[4]The Fourth Medical Center of China General Hospital of People's Liberation Army, China.

[*]Corresponding author: Yongli Yan, Beijing Advanced Innovation Center for Biomedical Engineering, Beihang University, China, e-mail address: yanyongli0318@buaa.edu.cn

Submitted: 19th October 2024

Accepted: 28th November 2024

Abstract

Purpose: Accurate biomechanical modeling is crucial for enhancing the realism of virtual surgical training. This study addresses the computational cost and complexity associated with traditional viscoelastic models by incorporating neural network algorithms, thereby augmenting the predictive capability of soft tissue modeling. *Methods:* To address these challenges, the present study proposes a novel biomechanical modeling approach. The approach establishes a relaxation prediction model based on the backpropagation (BP) neural network and optimizes it using an enhanced sparrow search algorithm (ISSA). This hybrid method leverages the dynamic characteristics of forceps to predict the relaxation force of soft tissues more accurately. The ISSA optimizes the model by integrating chaos mapping, nonlinear inertia weight, and vertical-horizontal crossover strategy, which helps overcome the issue of local optima and boosts the predictive performance. *Results:* The experimental results demonstrated that the R^2 values reached 0.9956 for the pig kidney and 0.9896 for the pig stomach, indicating the model's exceptional precision in predicting relaxation forces. *Conclusions:* The relaxation force prediction model based on ISSA-BP neural network provides excellent predictive performance, offering a new and effective strategy for biomechanical modeling of soft tissues in virtual surgical systems.

Keywords: Biomechanical modeling, viscoelasticity, relaxation force, neural network, sparrow search algorithm

1. Introduction

Virtual surgical systems are the most representative application of medical virtual reality technologies routinely used by surgeons for training, surgical planning, and simulation [2, 3]. Highly realistic virtual surgical environments greatly improves the training of lead surgeons [27]. However, due to the complexity of biomechanical modeling, existing virtual surgical systems mostly lack real-time and accurate force feedback making it difficult to be widely adopted [18].

Soft tissues are heterogeneous, anisotropic, nonlinear and viscoelastic [6, 16]. Viscoelasticity is a challenging aspect in biomechanical modeling as biological tissues exhibit both elastic solid and viscous fluid properties. Feng Yuanzhen [11], the pioneer of modern computational biomechanics, noted that almost all biological tissues exhibit viscoelastic behavior, only differing in their degree of elasticity or viscosity. Biological tissues, especially soft tissues, exhibit pronounced viscoelastic behavior because they are composed of materials such as elastic and collagen fibers [26]. Experiments on these materials have demonstrated widespread nonlinear stress-strain relationship, hysteresis during loading and unloading, and stress relaxation [12].

Current mainstream biomechanical modeling methods include spring damping, function and finite element methods. Spring damping model simulates viscoelasticity of soft tissues by connecting spring dampers in series and parallel[31-33]. The method of function fitting is mainly based on the constitutive equation and experimental data[5, 11, 35, 37]. The finite element method is used to compute complex mechanics problems by dividing the solution domain into multiple subdomains[4, 28]. However, each of these methods possesses inherent limitations. Spring damping models necessitate precise parameter tuning and often fail to accurately capture the complex nonlinear and time-dependent behavior of biological tissues. Function fitting methods, while simpler, heavily rely on accurate experimental data and may struggle with generalizing to unseen data. The finite element method, although powerful, entails high computational costs, extensive parameter calibration requirements, and challenges in fault tolerance, thereby limiting its real-time application in virtual surgical systems. These challenges impede the effectiveness of current models in providing real-time dynamic force feedback crucial for realistic virtual surgical environments.

To address these challenges, this study proposes a new approach that integrates neural network-based learning algorithms into biomechanical modeling. For this purpose, the pressure relaxation behavior of pig kidney and stomach tissue was used as a model. Firstly, stress relaxation experiments were conducted on pig kidneys and

stomach tissue to investigate the influence of clamping forceps motion parameters on the relaxation force. Subsequently, an improved sparrow search algorithm (ISSA) optimized back propagation (BP) neural network model was adopted to predict the relaxation force of the soft tissues. This approach introduced circular chaotic mapping, nonlinear inertia weight, and vertical-horizontal crossover into the sparrow search algorithm (SSA) to prevent the model from being trapped in local optimal solutions. This approach significantly improved the accuracy and stability of the prediction model. Finally, the accuracy of the model was validated through relaxation experiments. Taken together, the goal was to improve the universality and robustness of the model, simplify the parameter calculation process, avoid complex parameter fitting problems, and further optimize the biomechanical modeling of virtual surgical systems to improve its realistic experience. This would provide more reliable data support and technical assurance for lifelike simulation of surgical procedures.

2. Materials and methods

2.1 Experiment

2.1.1 Experimental materials

The pig kidneys and stomachs were obtained from slaughterhouses near the institution. The average weight of each pig was between 50-60kg with ages between 18-22 weeks. Freshly harvested pig kidneys and stomachs were transported in a portable refrigerator to the laboratory as quickly as possible. Pig kidney tissues were cut into pieces measuring approximately 30±1mm (L) x 15±1mm (W) x 8mm±1mm (D). The pig stomach tissues were trimmed into pieces measuring approximately 30±1mm (L) x 20±1mm (W) x 5mm±1mm (D) for easy compression treatment with the forceps. The processed samples were stored at 4 °C to prevent tissue dehydration or other issues.

2.1.2 Experimental equipment

The EZ-LX Compact Table-Top Universal / Tensile Tester (Shimadzu, Japan) (Figure 1) was used as the platform for this experiment. It was equipped with a force

sensor with an accuracy of 0.5% and a measurement range of 0-50N with an experimental indenter installed at the operating end. To study the effect of different clamp leaf areas on soft tissue relaxation force, three indenters with different sizes (Table 1), YT1, YT2, and YT3, were also used.

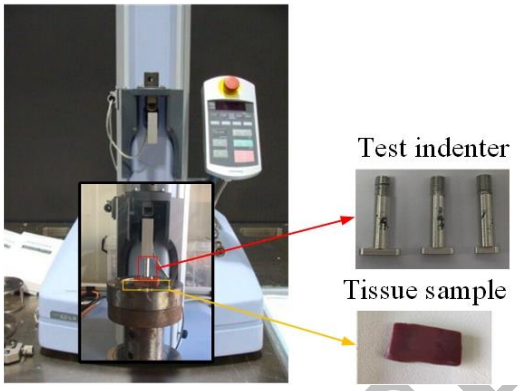

Figure 1 Apparatus for relaxation testing

Table 1 Types and dimensions of indenter

Type	Outline size (mm)	Groove size (mm)	Area (mm^2)	Tooth height (mm)	Tooth angle (°)
YT1	15.20*5.00	12.60*2.40	45.76	0.2	90
YT2	12.16*4.00	10.08*1.92	29.29		
YT3	9.12*3.00	7.56*1.44	16.47		

Table 2 Experimental parameters

Loading displacement	Pig kidney: 3mm, pig stomach: 2mm											
Type	YT1				YT2				YT3			
Velocity (mm/s)	0.5	1	1.5	2	0.5	1	1.5	2	0.5	1	1.5	2

2.1.3 Experimental design

The experimental parameters set were loading depth, initial loading speed and relaxation time. As the thicknesses of the processed pig kidney and stomach tissue samples were ~ 8mm and 5mm respectively, the loading depth for pig kidney tissues was set at 3mm, while for pig stomach tissues, it was set at 2mm. To simulate lifelike

surgical procedures, the initial loading speed parameters were set at 0.5mm/s, 1mm/s, 1.5mm/s, and 2mm/s. The indenters stayed in place for a relaxation time of 50s after reaching the designated loading depth. To facilitate visual analysis of factors affecting relaxation force, experimental groups were designed based on the controlled variable method (Table 2). A total of twelve experimental groups encompassing different relaxation times, initial loading speeds, and indenter contact areas (compression areas), divided into three comparative categories, were established.

2.2 Relaxation force prediction model

2.2.1 Improved sparrow search algorithm

SSA is a swarm intelligence optimization algorithm based on the foraging and anti-predator behavior of sparrows [34]. However, to obtain an ideal optimal solution poses a significant challenge for SSA in balancing local and global searches while avoiding getting trapped in local optima [21, 23, 36]. Therefore, this study introduced improvements to the SSA by incorporating circular chaotic mapping [17], nonlinear inertia weight, and vertical-horizontal crossover [24].

The principle of the improved sparrow search algorithm is as described: Firstly, population positions are initialized based on circular chaotic mapping. Traditional SSA generates an initial population using pseudo-random methods, which may lead to clustering of individuals and uneven distribution within the population [7]. By employing specific strategies that promote more random and uniform generation of initial individuals, both the quality of initial solutions and convergence speed can be significantly enhanced [7, 25]. We introduce an approach based on circular chaotic mapping to achieve a higher-quality initial population for our algorithm. Circular chaotic mapping is characterized by relative stability and high coverage rate of chaos values [1, 17]:

$$y_{i+1} = \mathrm{mod}\left(y_i + a - \frac{b}{2\pi}\sin\left(2\pi y_i\right), 1\right) \tag{1}$$

where $i = 1, 2, \cdots, n$, y_i is a chaotic sequence within the range of $[0 \quad 1]$, a and b are two control parameters, and mod is the modulo function [1].

The mapping is then used for population initialization in the following way:

$$x_{i,j} = lb + (ub - lb) \times y_i \tag{2}$$

where $x_{i,j}$ represents the value of the i^{th} sparrow in the j^{th} dimension, and *lb* and *ub* respectively represent the lower and upper bound of the search space for sparrows.

Secondly, the discoverer's position is updated using a nonlinear inertia weight to enhance the SSA algorithm, which struggles with step size control. This leads to rapid convergence towards optimal solutions, risking local optima. To improve global exploration and local exploitation, we introduce an adaptive inertia weight factor ω to control the search capability and range of discoverers, preventing them from getting trapped in local optima. The formula for calculating the adaptive inertia weight factor ω is as follows:

$$\omega = \exp\left(1 - \frac{t_{\max} + t}{t_{\max} - t}\right) \tag{3}$$

where $t_{\max}$ represents the maximum number of iterations, and *t* represents the current iteration count. With an increasing number of iterations, the weight factor ω underwent corresponding nonlinear changes. Through adaptive adjustment, the discoverer could accurately find the optimal solution. The improved method for determining the position of the discoverer is as follows [8].

$$X_{i,j}^{t+1} = \begin{cases} X_{i,j}^{t} * \omega & R_2 < ST \\ X_{i,j}^{t} + Q \cdot L & R_2 > ST \end{cases} \tag{4}$$

where *t* represents the current iteration value, *j* represents the dimension from 1 to d, $X_{i,j}^{t}$ represents the value of dimension *j* for sparrow *i* at iteration *t*, $R_2 \in [0,1]$ and $ST \in [0.5,1.0]$ represent the alarm value and safety threshold respectively. *Q* is a random number following a normal distribution, *L* represents a *1*d* matrix with all elements being 1. If $R_2 < ST$, then the sparrow population is safe. Otherwise, some sparrows perceive danger, and all sparrows must quickly move to a safe area.

In the third step to update the follower's position, the premise taken is that followers will constantly monitor the producer, and if they discover that the producer has better food, they will compete for it. If they win, they get the food, if not, they continue to monitor [34].

$$X_{i,j}^{t+1} = \begin{cases} Q \cdot \exp\left(\dfrac{X_{worst}^{t} - X_{i,j}^{t}}{j^2}\right) & i > n/2 \\ X_{p}^{t+1} + \left|X_{i,j}^{t} - X_{p}^{t+1}\right| \cdot A^{+} \cdot L & otherwise \end{cases} \tag{5}$$

where X_p^t represents the best position occupied by the producer, X_{worst}^t represents the current worst position, and A represents a 1*d matrix where elements are randomly assigned 1 or -1, with $A^{+} = A^{T}\left(AA^{T}\right)-1$ where T stands for matrix transpose . When $i>n/2$, the fitness value of the i^{th} follower is relatively poor indicating hunger.

Finally, the alert location is updated based on the crisscross strategy [8, 24] where the vertical and horizontal crossover strategy is introduced to improve the search method of the alerters, while maintaining convergence speed and enhancing solution accuracy. Horizontal crossing divides the solution space of multidimensional problems into semi-group hypercubes for edge searching, reducing blind spots and strengthening the algorithm's global optimization ability. Through vertical crossover, different dimensions in the population undergo crossover operations without affecting other dimensions, enabling dimensions that are stuck in local optima to break out. The algorithm is solved through competition and comparison between these two strategies.

The position updated formula of alerters after horizontal crossing is as follows:

$$MSx_{i,d}^{t} = r_1 \times x_{i,d}^{t} + (1 - r_1) \times x_{j,d}^{t} + c_1 \times \left(x_{i,d}^{t} - x_{j,d}^{t}\right) \tag{6}$$

$$MSx_{j,d}^{t} = r_2 \times x_{j,d}^{t} + (1 - r_2) \times x_{i,d}^{t} + c_1 \times \left(x_{j,d}^{t} - x_{i,d}^{t}\right) \tag{7}$$

where $MSx_{i,d}^{t}$ and $MSx_{j,d}^{t}$ are d-dimensional individuals generated by the lateral crossover of alerters $x_{i,d}^{t}$ and $x_{j,d}^{t}$. r_1 and r_2 are random numbers within [0,1], while c_1 and c_2 are random numbers within [-1,1]. Through lateral crossover, the offspring

individuals generated were compared with the parent individuals, and the optimal individual was retained based on their fitness values.

The position update formula of the alerter after vertical crossing is as follows:

$$MSx_{i,d}^{t} = r \times x_{i,d_1}^{t} + (1-r) \times x_{i,d_2}^{t} \tag{8}$$

where $MSx_{i,d}^{t}$ is the offspring individual generated by vertically crossing the d_1 and d_2 dimensions of individual $x_{i,d}^{t}$, and $r \in [0,1]$. As seen for horizontal crossing, the offspring individuals generated by vertical crossing operation competed with the parent generation which select individuals with higher fitness for preservation.

2.2.2 ISSA-BP neural network

BP neural network is an error backpropagation training algorithm for a multi-layer network structure, which includes input layer, hidden layer, and output layer [30]. Although the BP neural network has powerful nonlinear mapping capability and fault tolerance, its algorithm is prone to getting trapped in local optima [9]. Therefore, this study uses an improved SSA algorithm to optimize the weights and thresholds of the BP network (Figure 2). To predict the soft tissue relaxation force, we select contact area of the indenter, initial speed and time as input vectors; relaxation force as output data; and a network structure with only one hidden layer. The initial steps are (i) the architecture of the BP neural network was determined, and sample data collection is initialized, and (ii) population size, caution value, safety threshold, and number of iterations for the improved SSA are determined. The overall size of individuals is set based on preprocessed input data, where each individual consisted of weights and thresholds from the input layer to the hidden layer, as well as weights and thresholds from the hidden layer to the output layer. The following steps are then undertaken:

Step (iii): The discoverer's position is updated by recalculation using formula (4).

Step (iv): The follower's position is updated using formula (5).

Step (v): The alerter's position is updated using formulas (6)-(8).

Step (vi): The fitness of individuals is calculated in the newly generated population. If these requirements are met, the evolution was deemed completed; otherwise, steps 3-6 were repeated.

Step (vii): A BP neural network is constructed using the improved SSA optimization weights and thresholds and the training data are analyzed.

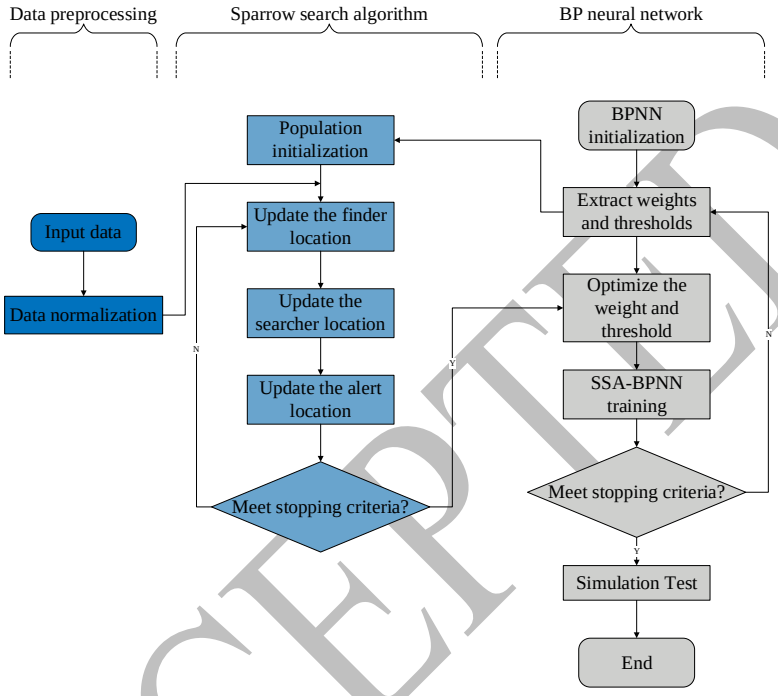

Figure 2 Flowchart of ISSA-BP Algorithm.

2.2.3 Validation indexes

To evaluate the prediction error and effectiveness of the model, Root Mean Square Error (RMSE), Mean Square Error (MSE), Mean Absolute Error (MAE), Sum of Squared Errors (SSE), and Coefficient of Determination (R^2) are used as evaluation metrics. Lower values for RMSE, MSE, MAE, and SSE indicate smaller prediction errors and better prediction performance, while R^2 reflects the correlation between predicted values and actual values, with larger R^2 values indicating better prediction performance. The formulas for calculating each evaluation metric are provided below.

$$RMSE = \sqrt{\frac{1}{n}\sum_{i=1}^{n}\left|y_i - o_i^{(L)}\right|^2} \tag{9}$$

$$MSE = \frac{1}{n}\sum_{i=1}^{n}\left|y_i - o_i^{(L)}\right|^2 \tag{10}$$

$$MAE = \frac{1}{n}\sum_{i=1}^{n}\left|y_i - o_i^{(L)}\right| \tag{11}$$

$$SSE = \sum_{i=1}^{n}\left(y_i - o_i^{(L)}\right)^2 \tag{12}$$

$$R^2 = 1 - \frac{\sum_{i=1}^{n}\left(o_i^{(L)} - y_i\right)^2}{\sum_{i=1}^{n}\left(y_i - \bar{y}\right)^2} \tag{13}$$

where $o_i^{(L)}$ represents the predicted output value, y_i represents the actual value, $\bar{y}$ is the mean of y_i, and N is the sample size.

To further analyze performance differences between models, this study also introduces F-test and confidence interval as auxiliary analysis tools. The F-test is used to compare the significant differences in variance among multiple models. The formula for the F-test is as follows:

$$F = \frac{\sum\left(\bar{Y}j - \bar{Y}\right)^2 / (k-1)}{SSE / (N-k)} \tag{14}$$

where $\bar{Y}j$ represents the average value of group *j*, $\bar{Y}$ represents the average value of all groups. *N* represents the total sample size, and *k* represents the number of groups. If the calculated *F* value is greater than the critical value, it indicates that there is a significant difference between at least one pair of models. The F-test helps us determine whether there is a statistically significant difference in the overall predictive performance of the models.

The confidence interval is used to estimate the range of model prediction errors. The formula for a 95% confidence interval is as follows:

$$CI = \bar{X} \pm Z_{\alpha/2} \times \frac{\sigma}{\sqrt{n}} \tag{15}$$

where $\bar{X}$ is the sample mean, σ is the sample standard deviation, *n* is the sample size, and $Z_{\alpha/2}$ is the critical value of the standard normal distribution (for a confidence level of 95%, $Z_{\alpha/2} = 1.96$).

3. Results

3.1 Factors influencing biological tissue relaxation force

3.1.1 Relaxation time

Experimental data revealed a force-time curve (Figure 3(a)) showing an initial drastic change in force that gradually smoothed out. A 0.02s sampling interval quantified this change (Figure 3(b)). The rate of force change was significant within the first 2s, stabilizing after 5s, indicating that the tissue reached a relatively stable relaxed state.

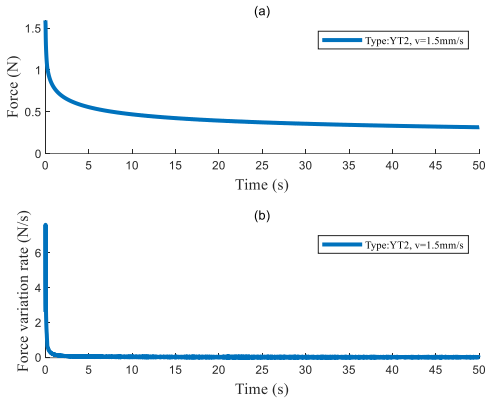

Figure 3 The force-time curve changes and the rate of change in the soft tissue relaxation test.

3.1.2 Initial speed

Relaxation experiments on pig kidney and stomach tissues provided comparative speed data, shown in Figure 4. Figures 4(a) and 4(b) present kidney tissue relaxation tests with indenter YT1 at varying speeds, while Figures 4(c) and 4(d) illustrate stomach tissue data. From Figures 4(a) and 4(c), it is evident that the higher initial speeds resulted in greater initial forces, indicating that high-speed compression led to higher initial stress on the tissues. Regardless of the speed, the force gradually decreased and stabilized over time; however, under high-speed conditions, the force achieved a larger stable force value. Figures 4(b) and 4(d) depict variations in force with time. During the early stage of relaxation (0-2s), there was a pronounced decline in the rate of relaxation force, whereby higher initial speeds leading to more rapid rates of decline. After about5s, stable relaxation force rate was observed across all test conditions.

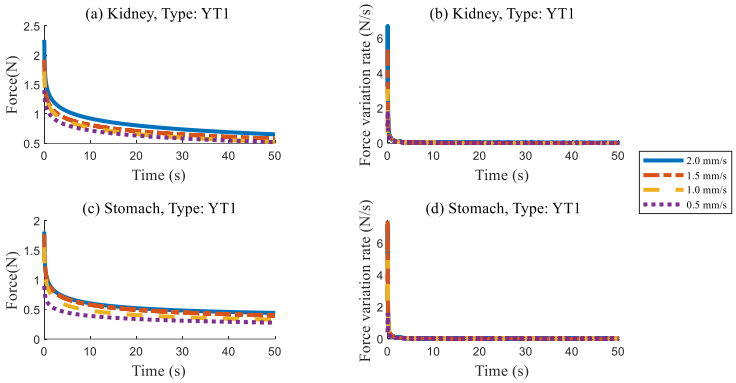

Figure 4 Comparison of soft tissue relaxation forces at different speeds.

3.1.3 Contact area

The indenter's contact area significantly influenced relaxation force. Figure 5 compares force-time curves across different contact areas. Figures 5(a) and 5(b) show kidney tissue relaxation experiments at 1.5 mm/s, while Figures 5(c) and 5(d) present stomach tissue results at 1.0 mm/s. With an increase in contact area, the initial force was greater and decreased more rapidly (Figure 5(a) and 5(c)). Over time, forces gradually decreased and stabilized, with larger contact areas yielding relatively higher stable force values.

On the other hand, Figures 5(b) and 5(d) demonstrate the rate of change in force calculated with a 0.02s interval. Within the first 2s, relaxation forces rapidly decreased, with larger contact areas leading to faster rates of decrease. After ~5s, under various contact area conditions, rates of change in relaxation force stabilized at lower values, indicating a relatively stable tissue state.

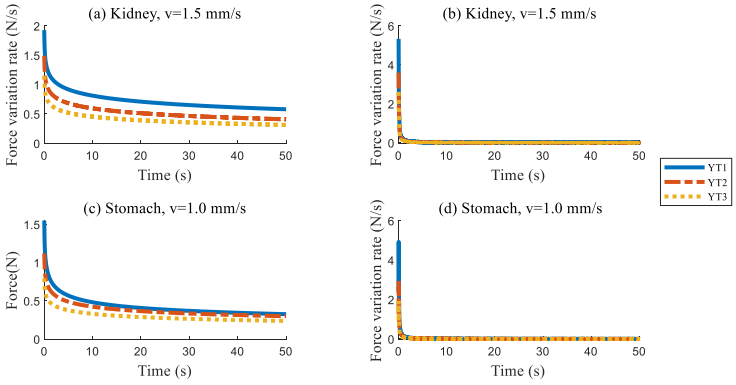

Figure 5 Comparison of soft tissue relaxation forces under different indenters.

3.2 Analysis of relaxation force prediction model

3.2.1. Comparison of model prediction performance

To verify the predictive performance of the ISSA-BP model, we compared it with the SSA-BP and traditional BP neural network models. Figures 6(a)-6(b) demonstrate the performance of these three models in predicting relaxation forces. Although all three models showed good predictive capabilities, the ISSA-BP model exhibited superior prediction ability in relaxation force, as its predicted values closely matched the actual relaxation curves.

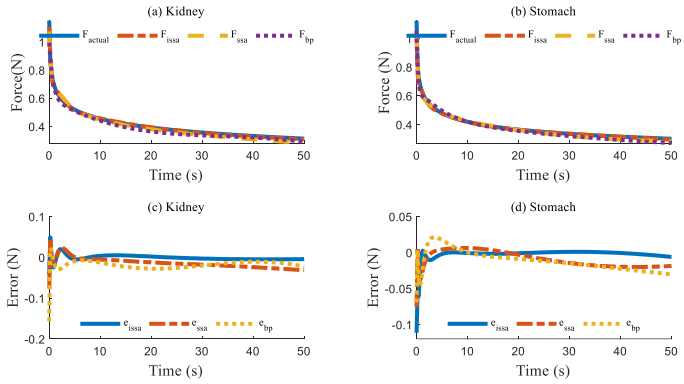

Figure 6 Comparison of relaxation force prediction results of ISSA-BP, SSA-BP and traditional BP models.

Figure 6 (c)-6(d) show the prediction errors of the three models. The ISSA-BP model exhibited fluctuations in prediction error during the initial stage but quickly converged to a value close to zero. However, the other two models consistently exhibited large fluctuations in prediction error, and even after relaxation stability was achieved, the error did not fully converge to zero. This suggested that the ISSA-BP model had significant superiority in predicting soft tissue relaxation force.

3.2.2. Analysis of error evaluation indicators

The error evaluation indexes of different models in predicting the relaxation force of pig kidney and pig stomach are presented in Table 3. The ISSA-BP model exhibits significant advantages across all error indicators (RMSE, MSE, MAE, SSE). For instance, the RMSE value for the ISSA-BP model in kidney tissue is 0.0068, significantly lower than the SSA-BP model (0.0192) and traditional BP model (0.0218).

Similarly, the ISSA-BP model achieved an RMSE of 0.0095 for gastric relaxation, outperforming the SSA-BP (0.0147) and BP (0.0181) model. The R^2 values for the ISSA-BP model were 0.9956 (pig kidney) and 0.9896 (pig stomach), indicating a strong agreement between predicted and actual data.

Table 3 Evaluation indicators of different models

		RMSE	MSE	MAE	SSE	R^2
kidney	BP	0.0218	0.0011	0.0189	0.1194	0.9541
	SSA-BP	0.0192	0.001	0.0169	0.0924	0.9645
	ISSA-BP	**0.0068**	**0.0003**	**0.0045**	**0.0115**	**0.9956**
stomach	BP	0.0181	0.001	0.0156	0.0825	0.9624
	SSA-BP	0.0147	0.0008	0.0119	0.0543	0.9753
	ISSA-BP	**0.0095**	**0.0005**	**0.0029**	**0.0227**	**0.9896**

Table 4 further validates the predictive accuracy of the ISSA-BP model through an F-test. The F-statistic shows that the prediction errors of the ISSA-BP model are significantly lower than that of the SSA-BP and BP models (pig kidney: F=185.89, p=0.0000; pig stomach: F=43.03, p=0.0000). The 95% confidence intervals for the ISSA-BP model are [-0.0012, -0.0013] (pig kidney) and [-0.0025, -0.0026] (pig stomach), which are significantly narrower compared to those of the SSA-BP and BP models, indicating smaller errors and higher stability for this model.

Table 4 F-test and 95% confidence interval results under three prediction models for pig kidney and pig stomach

		Pig kidney	Pig stomach
F-test	F-statistic	185.89	43.0335
	p-value:	0.0000	0.0000
Confidence Intervals	BP95%CI:	[-0.0185, -0.0186]	[-0.0117, -0.0118]
	SSA-BP 95% CI:	[-0.0145, -0.0146]	[-0.0094, -0.0095]
	ISSA-BP 95% CI	[-0.0012, -0.0013]	[-0.0025, -0.0026]

4. Discussion

4.1 Soft tissue relaxation

In this study, we developed the ISSA-BP neural network model for biomechanical modeling, which successfully predicted the relaxation behavior of soft tissues. Our analysis focused on key factors such as relaxation time, initial speed, and the contact area of the indenters, providing a deeper understanding of the mechanical behavior of soft tissues. Consistent with previous researches [10, 14, 15, 20, 29], we found that soft tissues exhibit strong time dependence during the relaxation phase (Figure 2). Furthermore, high-speed loading resulted in a rapid and significant force drop, indicating that speed affects peak forces during loading and influences the relaxation properties of force. These findings suggest that precise control of speed and contact area is crucial for optimizing surgical procedures.

The results of our study are consistent with previous research, indicating that both kidney and stomach tissues exhibit typical viscoelastic characteristics during the relaxation phase [14, 29]. Lu et al. [22] conducted relaxation tests on kidney tissues, but mainly compared soft tissue relaxation coefficients under different storage conditions. Li et al. [13, 19] discovered significant regional and interlayer heterogeneity in the relaxation stress of pig stomachs. However, most existing research has focused on single-loading mode experiments [10, 14, 15, 29], whereas our study uniquely indicates multiple factors affecting soft tissue relaxation, such as time, loading speed, and the contact area. This broader approach allows for a more comprehensive understanding of the biomechanical properties of soft tissues and sets our study apart in the field.

4.2 Model Development and Validation

To enhance the accuracy of relaxation behavior prediction, we have developed the ISSA-BP neural network model that integrates crucial dynamic factors including contact area, initial speed, and time. The performance of this model has been further improved through the implementation of the ISSA optimization algorithm, resulting in significant enhancements in both prediction accuracy and convergence speed. When compared to traditional BP neural networks and SSA-BP models, the ISSA-BP model

exhibits distinct advantages, particularly in terms of reducing error margins and enhancing prediction stability. The results showed that the ISSA-BP model significantly outperforms the SSA-BP model by reducing the RMSE by 64.6% in predicting porcine renal relaxation force, and by 68.8% compared to the traditional BP model. Similarly, the RMSE for porcine gastric relaxation force was reduced by 35.4% and 47.5%, respectively.

Furthermore, the enhanced R^2 value provides further evidence of the ISSA-BP model's ability to reflect the nonlinear behavior during soft tissue relaxation, thereby validating the effectiveness of ISSA optimization in enhancing predictive capability. Moreover, the F-test result ($p = 0.0000$) confirms that the error variance of the ISSA-BP model is significantly lower compared to both SSA-BP and BP models. The narrower and non-overlapping confidence intervals of the ISSA-BP model further emphasize its superiority in terms of prediction accuracy and reliability.

4.3 Limitations

While our study provided valuable insights, certain limitations should be noted. First, we analyzed factors like relaxation time, initial speed, and contact area, however we did not fully account for other complex influences such as tissue microstructure, blood flow, temperature changes, and patient physiology, which may affect predictive accuracy in real-life scenarios. Second, the model focused on predicting viscoelasticity but did not cover other biomechanical properties such as elasticity and shear modulus. This limitation restricts its broader applicability. Further research is needed to expand the model to other biomechanical fields.

5. Conclusion

This study successfully developed an ISSA-BP neural network for biomechanical modeling, which demonstrated excellent predictive capability for soft tissue relaxation, with good stability and accuracy. By analyzing the effects of relaxation time, initial speed, and contact area of the indenters, we enhanced the understanding of soft tissue

mechanical behavior, which is essential for improving the application of virtual surgical systems.

In the future, further optimization of the model parameters will be performed with a wider range of biological tissue types while exploring the possibility of incorporating deep learning techniques to achieve broader clinical applications and improvements in educational training tools.

Funding: This paper is supported by National Natural Science Foundation of China under grant No. 52305066.

References

[1] Arora S, Anand P. Chaotic grasshopper optimization algorithm for global optimization. NEURAL COMPUT APPL 2019, 31: 4385-4405, https://doi.org/10.1007/s00521-018-3343-2

[2] Barr ML, Haveles CS, Rezzadeh KS, Nolan IT, Castro R, Lee JC, Steinbacher D, *et al.* Virtual surgical planning for mandibular reconstruction with the fibula free flap: a systematic review and meta-analysis. ANN PLAS SURG 2020, 84: 117-122, https://doi.org/10.1007/s00521-018-3343-2

[3] Bhandari K, Lin C-H, Liao H-T. Secondary mandible reconstruction with computer-assisted-surgical simulation and patient-specific pre-bent plates: the algorithm of virtual planning and limitations revisited. Applied Sciences 2022, 12: 4672, https://doi.org/10.3390/app12094672

[4] Brouwer I, Mora V, Laroche D. A viscoelastic soft tissue model for haptic surgical simulation. Second Joint EuroHaptics Conference and Symposium on Haptic Interfaces for Virtual Environment and Teleoperator Systems (WHC'07)ed.: IEEE 2007: 593-594

[5] Calvo-Gallego JL, Domínguez J, Cía TG, Ciriza GG, Martínez-Reina J. Comparison of different constitutive models to characterize the viscoelastic properties of human abdominal adipose tissue. A pilot study. J MECH BEHAV BIOMED 2018, 80: 293-302, https://doi.org/10.1016/j.jmbbm.2018.02.013

[6] Chanda A, Callaway C. Tissue anisotropy modeling using soft composite materials. APPL BIONICS BIOMECH 2018, 2018: 4838157, https://doi.org/10.1155/2018/4838157

[7] Dokeroglu T, Sevinc E, Kucukyilmaz T, Cosar A. A survey on new generation metaheuristic algorithms. COMPUT IND ENG 2019, 137: 106040, https://doi.org/10.1016/j.cie.2019.106040

[8] Duan Y, Liu C. Sparrow search algorithm based on Sobol sequence and crisscross strategy. Journal of Computer Applications 2022, 42: 36,

[9] Duan Y, Mu C, Yang M, Deng Z, Chin T, Zhou L, Fang Q. Study on early warnings of strategic risk during the process of firms' sustainable innovation based on an optimized genetic BP neural networks model: evidence from Chinese manufacturing firms. INT J PROD ECON 2021, 242: 108293, https://doi.org/10.1016/j.ijpe.2021.108293

[10] Friis SJ, Hansen TS, Poulsen M, Gregersen H, Brüel A, Nygaard JV. Biomechanical properties of the stomach: A comprehensive comparative analysis of human and porcine gastric tissue. J MECH BEHAV BIOMED 2023, 138: 105614, https://doi.org/10.1016/j.jmbbm.2022.105614

[11] Fung Y-c. Biomechanics: mechanical properties of living tissues. Springer Science & Business Media 2013

[12] Haslach Jr HW. Nonlinear viscoelastic, thermodynamically consistent, models for biological soft tissue. BIOMECH MODEL MECHAN 2005, 3: 172-189, https://doi.org/10.1007/s10237-004-0055-6

[13] Holzer CS, Pukaluk A, Viertler C, Regitnig P, Caulk AW, Eschbach M, Contini EM, *et al.* Biomechanical characterization of the passive porcine stomach. ACTA BIOMATER 2024, 173: 167-183, https://doi.org/10.1016/j.actbio.2023.11.008

[14] Jia Z, Li W, Zhou Z. Mechanical characterization of stomach tissue under uniaxial tensile action. J BIOMECH 2015, 48: 651-658, https://doi.org/10.1016/j.jbiomech.2014.12.048

[15] Julie FS, Strøm HT, Mette P, Hans G, Vinge NJ. Dynamic viscoelastic properties of porcine gastric tissue: effects of loading frequency, region and direction. J BIOMECH 2022, 143: 111302, https://doi.org/10.1016/j.jbiomech.2022.111302

[16] Khan H, Abbasi SJ, Lee MC. DPSO and inverse jacobian-based real-time inverse kinematics with trajectory tracking using integral SMC for teleoperation. IEEE ACCESS 2020, 8: 159622-159638,

[17] Khan M, Masood F. A novel chaotic image encryption technique based on multiple discrete dynamical maps. MULTIMED TOOLS APPL 2019, 78: 26203-26222, https://doi.org/10.1007/s11042-019-07818-4

[18] Lesch H, Johnson E, Peters J, Cendán JC. VR simulation leads to enhanced procedural confidence for surgical trainees. J SURG EDUC 2020, 77: 213-218, https://doi.org/10.1016/j.jsurg.2019.08.008

[19] Li F, Liu J, Liu X, Wu Y, Qian L, Huang W, Li Y. Comparison of the Biomechanical Properties between Healthy and Whole Human and Porcine Stomachs. Bioengineering 2024, 11: 233, https://doi.org/10.3390/bioengineering11030233

[20] Li J, Bi X, Zhang K, Zhang C, Liu H. Experimental study on the effects of shear stress on viscoelastic properties of the intestines. SCI CHINA TECHNOL SC 2019, 62: 1028-1034, https://doi.org/10.1007/s11431-018-9428-4

[21] Liu Z, Hu C, Xiang T, Hu P, Li X, Yu J. A Novel Sparrow Search Scheme Based on Enhanced Differential Evolution Operator. IEEE T Em Top Comp I 2024, 10.1109/TETCI.2024.3437202

[22] Lu Y-C, Untaroiu CD. Effect of storage methods on indentation-based material properties of abdominal organs. P I MECH ENG H 2013, 227: 293-301, https://doi.org/10.1177/0954411912468558

[23] Ma J, Hao Z, Sun W. Enhancing sparrow search algorithm via multi-strategies for continuous optimization problems. INFORM PROCESS MANAG 2022, 59: 102854, https://doi.org/10.1016/j.ipm.2021.102854

[24] Meng A-b, Chen Y-c, Yin H, Chen S-z. Crisscross optimization algorithm and its application. KNOWL-BASED SYST 2014, 67: 218-229, https://doi.org/10.1016/j.knosys.2014.05.004

[25] Mirjalili S, Gandomi AH. Chaotic gravitational constants for the gravitational search algorithm. APPL SOFT COMPUT 2017, 53: 407-419, https://doi.org/10.1016/j.asoc.2017.01.008

[26] Nordsletten D, Capilnasiu A, Zhang W, Wittgenstein A, Hadjicharalambous M, Sommer G, Sinkus R, *et al.* A viscoelastic model for human myocardium. ACTA BIOMATER 2021, 135: 441-457, https://doi.org/10.1016/j.actbio.2021.08.036

[27] Pedram S, Kennedy G, Sanzone S. Toward the validation of VR-HMDs for medical education: a systematic literature review. VIRTUAL REAL-LONDON 2023, 27: 2255-2280, https://doi.org/10.1007/s10055-023-00802-2

[28] Qiang B, Greenleaf J, Oyen M, Zhang X. Estimating material elasticity by spherical indentation load-relaxation tests on viscoelastic samples of finite thickness. IEEE T ULTRASON FERR 2011, 58: 1418-1429, 10.1109/TUFFC.2011.1961

[29] Rosen J, Brown JD, De S, Sinanan M, Hannaford B. Biomechanical properties of abdominal organs in vivo and postmortem under compression loads. J BIOMECH ENG-T ASME 2008, https://doi.org/10.1115/1.2898712

[30] Rumelhart DE, Hinton GE, Williams RJ. Learning representations by back-propagating errors. nature 1986, 323: 533-536, https://doi.org/10.1038/323533a0

[31] Sopakayang R, De Vita R. A mathematical model for creep, relaxation and strain stiffening in parallel-fibered collagenous tissues. MED ENG PHYS 2011, 33: 1056-1063, https://doi.org/10.1016/j.medengphy.2011.04.012

[32] Takács Á, Rudas IJ, Haidegger T. Surface deformation and reaction force estimation of liver tissue based on a novel nonlinear mass–spring–damper viscoelastic model. MED BIOL ENG COMPUT 2016, 54: 1553-1562, https://doi.org/10.1007/s11517-015-1434-0

[33] Xu S, Liu XP, Zhang H, Hu L. A nonlinear viscoelastic tensor-mass visual model for surgery simulation. IEEE T Instrum Meas 2010, 60: 14-20, 10.1109/TIM.2010.2065450

[34] Xue J, Shen B. A novel swarm intelligence optimization approach: sparrow search algorithm. SYST SCI CONTROL ENG 2020, 8: 22-34, https://doi.org/10.1080/21642583.2019.1708830

[35] Ye X, Zhang J, Li P, Wang T, Guo S. A fast and stable vascular deformation scheme for interventional surgery training system. BIOMED ENG ONLINE 2016, 15: 1-14, https://doi.org/10.1186/s12938-016-0148-3

[36] Zhang J, Li L, Zhang H, Wang F, Tian Y. A novel sparrow search algorithm with integrates spawning strategy. CLUSTER COMPUT 2024, 27: 1753-1773, https://doi.org/10.1007/s10586-023-04036-4

[37] Zhang W, Chen HY, Kassab GS. A rate-insensitive linear viscoelastic model for soft tissues. BIOMATERIALS 2007, 28: 3579-3586, https://doi.org/10.1016/j.biomaterials.2007.04.040